Journal of Dental Sciences 19 (2024) 568–579

Available online at www.sciencedirect.com

ScienceDirect

journal homepage: www.e-jds.com

Original Article

Silica-based silver nanocomposite 80S/Ag as *Aggregatibacter actinomycetemcomitans* inhibitor and its *in vitro* bioactivity

Jung-Chang Kung [a,b,c,d], Tsung-Ying Yang [e,f,g,h], Chun-Cheng Hung [a,i**], Chi-Jen Shih [d,j,k*]

[a] *School of Dentistry, College of Dental Medicine, Kaohsiung Medical University, Kaohsiung, Taiwan*
[b] *Department of Clinical Dentistry, Kaohsiung Medical University Hospital, Kaohsiung, Taiwan*
[c] *Department of Dentistry, Kaohsiung Municipal Ta-Tung Hospital, Kaohsiung, Taiwan*
[d] *Drug Development and Value Creation Research Center, Kaohsiung Medical University, Kaohsiung, Taiwan*
[e] *Department of Medical Laboratory Science, I-Shou University, Kaohsiung, Taiwan*
[f] *Research Organization for Nano and Life Innovation, Future Innovation Institute, Waseda University, Tokyo, Japan*
[g] *Research Institute for Science and Engineering, Waseda University, Tokyo, Japan*
[h] *School of Education, Waseda University, Tokyo, Japan*
[i] *Division of Prosthodontics, Department of Dentistry, Kaohsiung Medical University Hospital, Kaohsiung, Taiwan*
[j] *Department of Fragrance and Cosmetic Science, College of Pharmacy, Kaohsiung Medical University, Kaohsiung, Taiwan*
[k] *Department of Medical Research, Kaohsiung Medical University Hospital, Kaohsiung, Taiwan*

Received 24 August 2023; Final revision received 11 October 2023
Available online 25 October 2023

KEYWORDS
Aggregatibacter actinomycetemcomitans;
Periodontitis;
Silica-based silver nanocomposite;
Silver

Abstract *Background/purpose:* As a commonly-found pathogen in periodontal disease, *Aggregatibacter actinomycetemcomitans* has been reported with several antibiotic resistance. Thus, to develop an alternative and protective therapy for *A. actinomycetemcomitans* infections is urgently needed in dentistry. In this study, we sought to synthesize a silica-based material to deliver silver nanoparticles for antibacterial purposes. Also, the bioactivities were examined via analyzing the formation of hydroxyapatite.
Materials and methods: The 80S/Ag powders were prepared by the evaporation-induced self-assembly method, with Si, Ca, P, and Ag composition ratios of 80, 15, 5, and 1/5/10 (mole

* Corresponding author. Department of Fragrance and Cosmetic Science, College of Pharmacy, Kaohsiung Medical University, No. 100, Shih-Chuan 1st Road, Sanmin Dist., Kaohsiung, 80708, Taiwan.
** Corresponding author. Division of Prosthodontics, Department of Dentistry, Kaohsiung Medical University Hospital, No. 100, Shih-Chuan 1st Road, Sanmin Dist., Kaohsiung, 80708, Taiwan.
E-mail addresses: chuchh@kmu.edu.tw (C.-C. Hung), cjshih@kmu.edu.tw (C.-J. Shih).

https://doi.org/10.1016/j.jds.2023.10.014

percentage), respectively. The nitrogen adsorption-desorption isotherms, transmission electron microscope, selected area electron diffraction, and Fourier transform infrared spectroscopy were conducted for textural analyses. The disk diffusion test was carried out against *A. actinomycetemcomitans* strain ATCC 29523. *In vitro* bioactivity assessment involved soaking 80S/Ag membrane powders in acellular simulated body fluid.

Results: We successfully developed a material consisting of Si, Ca, P, and Ag, namely the 80S/Ag. In the antibacterial testing, the 80S/Ag demonstrated antibacterial activity against the commonly-found oral pathogen, *A. actinomycetemcomitans*, with a long-lasting effect for 168h. The formation of hydroxyapatite in simulated body fluid highlighted the characteristic of dentine remineralization for the 80S/Ag. The increased pH values after immersion in simulated body fluid would help neutralize the acidic oral environment.

Conclusion: Our results indicate that 80S/Ag possesses remarkable antibacterial properties, hydroxyapatite formation, and increased pH values after immersion in simulated body fluid, supporting the potential therapeutic application of 80S/Ag for treating periodontal disease.

Introduction

Aggregatibacter actinomycetemcomitans (formerly *Actinobacillus actinomycetemcomitans*) is a gram-negative, facultatively anaerobic, and rod-shaped normal oral flora in humans.[1] If left untreated or treated inappropriately, *A. actinomycetemcomitans* could invade periodontal tissues, trigger inflammatory responses, and destroy the tooth-supporting tissues.[1] The formation of biofilms and the production of toxins contribute to the pathogenicity of *A. actinomycetemcomitans* and the development of aggressive periodontitis.[1] The diagnosis for *A. actinomycetemcomitans* included clinical examination, microbial testing, and molecular detection, which usually takes a long time to specify the pathogen.[1] The treatment for *A. actinomycetemcomitans* infections involves thorough mechanical cleaning accompanied by antibiotic therapy.[2] However, the previous study has reported instances of antibiotic-resistant *A. actinomycetemcomitans*, especially to amoxicillin, azithromycin, and metronidazole.[3] Thus, to develop an alternative and protective therapy for *A. actinomycetemcomitans* infections is urgently needed in clinical settings.

Periodontal diseases were usually led by several pathogens; e.g., *A. actinomycetemcomitans* might not be the sole cause.[4] Oral pathogens were diverse and included both gram-positive and gram-negative bacteria.[5] To this end, a broad-spectrum antimicrobial agent would be more suitable to develop a novel therapy for oral diseases, where silver meets the requirement and has been widely used.[6] Given its robust antibacterial property, silver has been used in multiple medical applications, such as wound care, tissue engineering, and antibacterial therapies.[7] Although the multi-way mechanism of action of silver against bacteria enhanced the antibacterial activities and lowered the risk of resistant development,[8] the hard-to-control concentration of silver led to toxicity.[8] Some efforts have been made for the antibacterial activity of silver against *A. actinomycetemcomitans*.[9,10] Parizi et al. reported a combination of silver nitrate with stomium acetate, with a lowered cytotoxicity to NIH3T3 cell line, a boosted antibacterial activity against *A. actinomycetemcomitans*, and thus, an increased therapeutical window for silver ion.[10] In another study, Wang et al. reported the titanium implant coating with silver-containing materials, representing antibacterial abilities against *A. actinomycetemcomitans* and *Streptococcus mutans*.[9]

Owing to the uniform pore sizes, large pore volumes, and large surface areas, mesoporous materials as a drug delivery system have attracted many researchers' interest.[11] Neither too large nor too small pores help control the release of the therapeutic substance inside, namely a controllable release system. Also, the characteristic of pores could enhance the exchanges of substrates or cell signals, helping the regeneration of lesions. Previous studies have announced that the mesoporous silica-based nanocomposites doped with silver nanoparticles would exhibit antibacterial activities against *Staphylococcus aureus*, *Escherichia coli*, *Klebsiella pneumoniae*, and *Pseudomonas aeruginosa*.[12–14] In a previous study, Gargiulo et al. reported a strong antibacterial effect of their Ag-containing mesoporous material against *S. aureus*, with a minimum inhibitory concentration of 0.5 mg/ml (solid-liquid ratio).[12] Zhu et al. modified the Ag-containing mesoporous material with amino acid and silane, designated as the Ag-SM58S material, which demonstrated strong and long-lasting antibacterial activities against both *E. coli* and *S. aureus*.[13] Yang et al. assessed the *in vitro* and *in vivo* activities of an Ag-containing mesoporous material against carbapenem-resistant *K. pneumoniae*.[15] Their result revealed that the Ag-containing mesoporous material possessed low cytotoxicity to the NIH3T3 cell line, solid antibacterial effect against carbapenem-resistant *K. pneumoniae*, and potential therapeutic effect in an infected *Caenorhabditis elegans* animal model. In this study, we sought to synthesize a silica-based material to deliver silver nanoparticles for antibacterial purposes. Also, the bioactivities were examined via analyzing the formation of hydroxyapatite.

Materials and methods

Materials preparation

The 80S/Ag powders with different silver molar ratios were prepared by the evaporation-induced self-assembly (EISA) method.[11] The 80S/Ag materials belong to the SiO_2—CaO—P_2O_5 system, with Si, Ca, and P composition ratios of 80, 15, and 5 (mole percentage), respectively. Various mole percentages of silver were added into the preparation, reneging from 0.0001 to 10 mol%. Briefly, the poly (alkylene oxide) block copolymer Pluronic F127 ($EO_{106}PO_{70}EO_{106}$) (BASF, Frankfurt, Germany) in 2 M nitric acid (ethanol) (Showa, Osaka, Japan) was mixed with precursors, including tetraethyl orthosilicate (TEOS) (Acros, NJ, USA), calcium nitrate tetrahydrate (Showa), triethyl phosphate (TEP) (Fluka, NC, USA) and silver nitrate (Showa). The solution was stirred for 1 d at room temperature, and then the gelation was performed using polyurethane foam (PUF) (NANPAO, Kaohsiung, TW) as a template. The thermal treatment was conducted at 600 °C for 2h to remove the precursors and form the porous scaffold. The Ag ratio of 0, 1, 5, and 10 were prepared and designated as 80S, 80S/Ag1, 80S/Ag5, and 80S/Ag10, respectively.

Textural characterization

To verify the effect of the growth of silver crystals on the porosity of the matrix, nitrogen adsorption-desorption isotherms were recorded.[12] The specific surface area of the samples was calculated with the Brunauer—Emmett—Teller (BET) equation and built-in Barret— Joyner—Halenda (BJH) method on the instrument (ASAP 2010, Micromeritics, USA). Nitrogen was used as an adsorbent. The specific surface areas, pore volume, and pore size of each 80S/Ag were tested using five test samples.

Transmission electron microscope (TEM) and selected area electron diffraction (SAED) examinations were conducted on the 80S/Ag test samples. The thickness of the 80S/Ag test samples must be sufficiently thin (<500 nm) and uniform to allow the electrons can penetrate them. In this study, the model of the TEM was JEM-2100 (JEOL, Japan). The TEM was used for observing the internal mesoporous structures, the internal mesoporous channels, the embedded silver particle circumstances, and the correlation between silver content and particle scale of the test 80S/Ag test samples. TEM specimens were prepared by dispersing the 80S/Ag powders in acetone in an ultrasonic bath for 5min. A drop of each suspension was cast onto a holey carbon film grid to prepare the specimens, and the solvent was evaporated for more than one week.

Fourier transform infrared spectroscopy (FTIR) and crystalline phases analysis

FTIR (Nicolet 6700, Thermo, USA) was used to investigate silver nitrate loading on the silica-based matrix's structural change. The 80S/Ag test samples were mixed with KBr at a mass ratio 1:10 and pressed into 200 mg pellets having a diameter of 12 mm. The FTIR absorption spectra were obtained with a frequency range of 400—4000 cm^{-1}, a spectral resolution 4 cm^{-1}, and an average of 64 scans. The FTIR absorption spectra for each sample were normalized by the spectrum of a blank KBr pellet. The crystalline phases of the powders of 80S/Ag0, 80S/Ag1, 80S/Ag5, and 80S/Ag10 were characterized by XRD patterns using an X-ray diffractometer (XRD-6000, Shimadzu, Japan) with Cu Kα radiation ($\lambda = 1.5418$ Å) and a Ni filter. The scan conditions were 30 kV and 20 mA with a scanning speed of 4°/min within the 2θ range of 10—80°.

Disk diffusion test

0.05g of the 80S/Ag powder was pressed into a disk using a hydraulic machine with 2000 pa pressure for 30s. The resulting disk was autoclaved and dried at 60 °C for 24h. A single colony of A. actinomycetemcomitans strain ATCC 29523 on a blood agar plate was suspended in brain-heart infusion (BHI) broth and adjusted to McFarland = 0.5. The bacterial suspension was then plated onto a tryptone soy agar plate to form the bacterial lawn, and the disks were placed onto the plate using sterilized tweezers. The plate was incubated at 37 °C under 5 % CO_2 for 48h. The diameter of the inhibition zone (clear zone) was measured. All experiments were performed in triplication.

In vitro bioactivity of 80S/Ag

In vitro bioactivity assessment involved soaking 80S/Ag membrane powders in acellular simulated body fluid (SBF) prepared according to the protocol proposed by Kokubo et al.[13] The different time frames for the analysis were 24, 48, 72, and 168 h. Then, the morphology of newly formed hydroxyapatite on the sample surface was observed with SEM (Hitachi S—3000 N, Hitachi, Tokyo, Japan). The mineral composition and crystal structure of hydroxyapatite was characterized by XRD (XRD-6000, Shimadzu, Japan) and Fourier transform infrared spectroscopy (Nicolet 6700, Thermo, USA).

Results

Textural analyses of the 80S/Ag

An X-ray diffraction analysis revealed the crystallization and types of 80S/Ag synthesized (Fig. 1). The diffraction peaks of the 80S/Ag were observed at 2θ = 38.1°, 44.3°, 64.5°, and 77.4°. After comparing with the JCPDs database, it was found to be the crystallization of face-centered cubic silver (Silver, JCPD 87—0597), with crystal planes of (111), (200), (220), and (311).[14] The crystalline intensity increased with the addition of silver. $CaSiO_3$ crystals were observed at 2θ = 29.4° in the 80S powder.[15] A broad peak was observed at 2θ < 30°, suggesting the crystalline structure of the scaffold with low crystalline intensity. With the increase in silver content, the diffraction peak of the scaffold became less prominent due to the more vigorous crystalline intensity of silver. Fourier-transform infrared spectroscopy (FTIR) was used to determine the functional groups of the samples based on specific wavelength absorption peaks

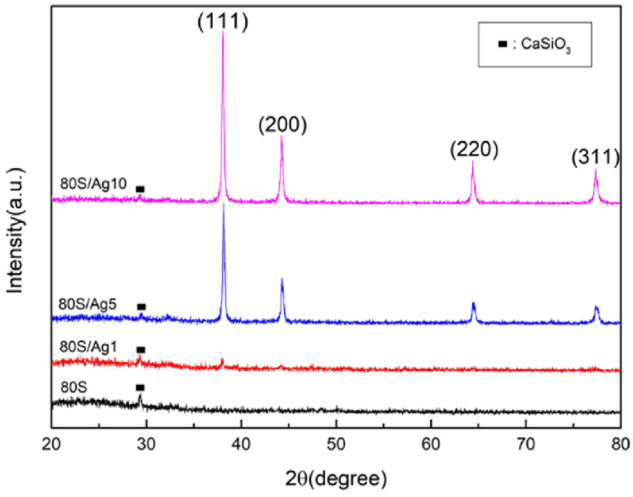

Figure 1 XRD patterns of 80S, 80S/Ag1, 80S/Ag5 and 80S/Ag10.

(Fig. 2). Absorption peaks of Si–O–Si and P–O–P were observed in the 1000-2000 cm^{-1} range in 80S, corresponding to the asymmetric stretching vibration.[16] The 725-800 cm^{-1} peaks indicated the symmetric stretching vibration of Si–O–Si, and those at 450-470 cm^{-1} represented the bending vibration of Si–O and P–O.[16] The absorption peaks of the 80S/Ag were similar to those of the 80S, indicating that the addition of silver did not affect the bonds in the wavelength range of 400–2000 cm^{-1}.

The results of nitrogen adsorption/desorption analysis for the 80S and 80S/Ag are shown in (Table 1) and (Fig. S1). All materials exhibit hysteresis loops in their adsorption/desorption results, which belonged to Type IV, H1 hysteresis curves commonly found in mesoporous materials (Fig. S1).[17] With an increase in the addition of silver, it can be observed that the adsorption curve of the 80S/Ag10 has decreased significantly, indicating a considerable reduction in surface area (Table 1) and (Fig. S1). The calculation results using the BET and BJH equations are shown in (Table 1). Due to

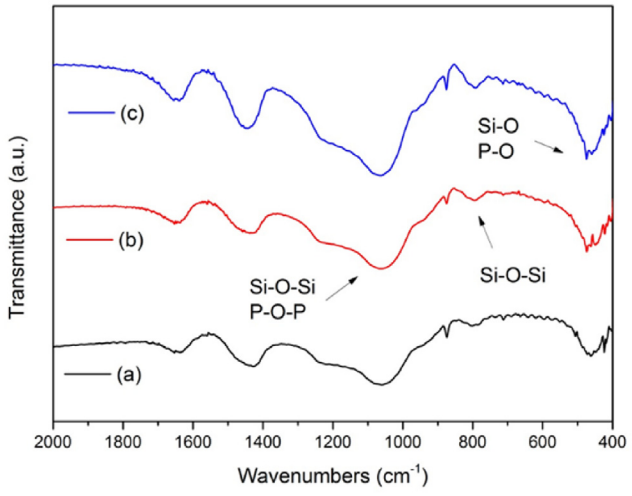

Figure 2 FTIR spectra of (a) 80S/Ag1, (b) 80S/Ag5, and (c) 80S/Ag10.

Table 1 BET results of 80S and 80S/Ag materials.

	Surface area (m^2/g)	Pore volume (cm^3/g)	Pore size (nm)
80S	348.9	0.72	7.3
80S/Ag1	307.6	0.60	7.5
80S/Ag5	280.0	0.46	6.6
80S/Ag10	264.5	0.41	6.2

mesoporous structures, the specific surface area and pore volume of 80S/Ag1, 80S/Ag5, and 80S/Ag10 gradually decrease with increasing silver content.

Comparing 80S/Ag10 and 80S (Fig. S1), the angle of 80S/Ag expands outward, suggesting that certain substances may have clogged the pores and led to less gas desorption. The result agreed with the crystalline morphology observed in XRD, indicating silver doped within the structure. High surface areas were found for 80S/Ag1, 80S/Ag5, and 80S/Ag10, with 307.6 m^2/g, 280.0 m^2/g, and 264.5 m^2/g, respectively. The pore size of the 80S/Ag decreases with increasing silver content, possibly due to silver adsorption within the mesopore windows, resulting in a reduction in pore size.

The powders of 80S/Ag1, 80S/Ag5, and 80S/Ag10 were observed using transmission electron microscopy (TEM) (Fig. 3). The uniform sizes and shapes of the 80S/Ag materials were observed and arranged orderly. The tiny black dots smaller than 7 nm were found inside the mesopores, indicating the silver crystals. The larger black dots outside the pores were also speculated as silver crystals, with the sizes tending to increase with an increase in silver content. The 80S/Ag1 was subjected to selected area electron diffraction (SAED) (Fig. 3d). According to the JCPDS database,[14] the face-centered cubic silver crystal structure on the (111) plane (Silver, JCPD 87–0597) was noted, which agreed with the XRD results. The result indicated that silver crystals were formed inside and outside the pores when adding silver with the 80S precursors in a loaded manner. The 80S/Ag1 was observed with silver crystals in the pore periphery, speculating that the addition of 1 mol% silver content may result in an excessive loading on 80S. To this end, less silver was examined to synthesize the 80S/Ag materials at 0.1, 0.01, and 0.001 mol%. The morphologies of 80S/Ag0.1, 80S/Ag 0.01, and 80S/Ag 0.001, were observed using TEM (Fig. S2). The micrographs revealed the ordered and well-arranged pores, whereas the silver particles were barely seen (Fig. S2a), likely due to the low silver amount. In the 80S/Ag0.01, a more significant number of small-sized silver nanoparticles can be observed; an increased number of silver particles within the mesopores was observed in the 80S/Ag0.1, with a few aggregations of silver particles found.

The surface morphology of 80S/Ag1, 80S/Ag5, and 80S/Ag10 was observed using SEM (Fig. 4). Spherical structures were noticed in all materials, and the sizes and amounts increased along with the silver content. The 80S/Ag10 exhibited distinct spherical structures with a diameter of approximately 500 nm. The following EDX elemental analysis revealed the strong signal of silver on the surface of the

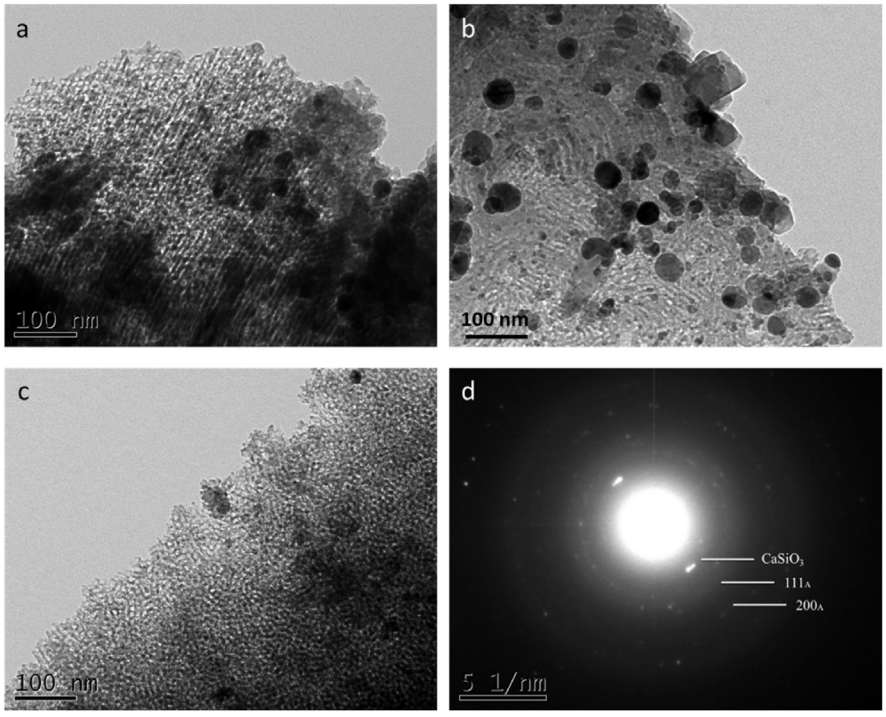

Figure 3 TEM micrographs of (a) 80S/Ag1, (b) 80S/Ag5, (c) 80S/Ag10, and SAED of (d) 80S/Ag10. A : Silver (JCPDs 87—0597).

spherical structures, indicating that the surface of the 80S/Ag10 was covered with silver particles, consistent with the TEM results.

Anti-*A. actinomycetemcomitans* activity of 80S/Ag

The antibacterial effect of 80S/Ag was evaluated against a common periodontal disease pathogen, *A. actinomycetemcomitans*, strain ATCC 29523. The inhibition zones could be observed for 80S/Ag1, 80S/Ag5, and 80S/Ag10 (Fig. 5), with 16.5-, 15-, and 15-mm diameters, respectively (Table 2). The smaller inhibition zone was noted for the materials containing lower silver (80S/Ag0.1, 80S/Ag 0.01, and 80S/Ag 0.001) as the lower silver decreased (Table S1). The dependence of the inhibition zone size on the silver content between 0.001 mol% and 10 mol% was visualized in (Fig. 6). Among all regimens, 1 mol% silver, namely the 80S/Ag1, resulted in the best antibacterial activity against *A. actinomycetemcomitans*, with a 16.5-mm inhibition zone. The tiny-sized silver particle would help the release rate,

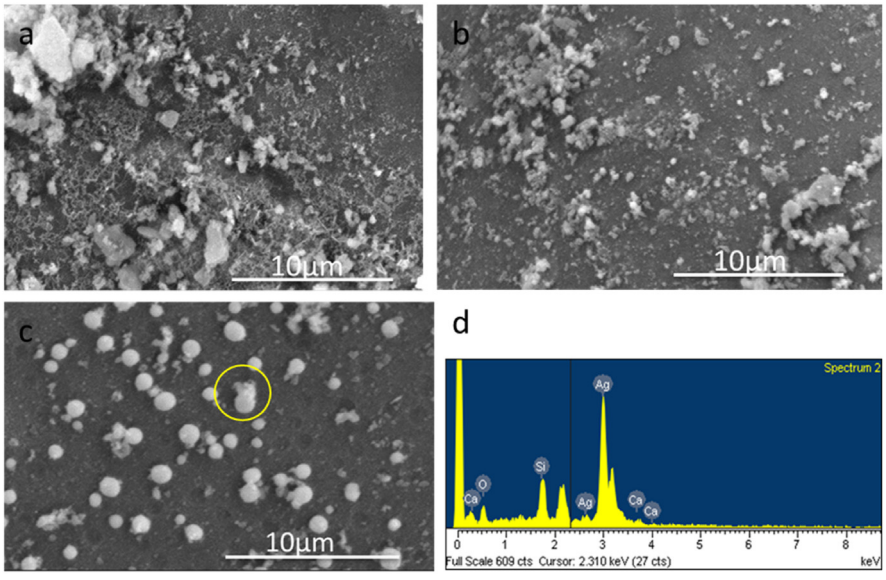

Figure 4 SEM micrographs of (a) 80S/Ag1, (b) 80S/Ag5, (c) 80S/Ag10 and (d) the EDS of the indicated location.

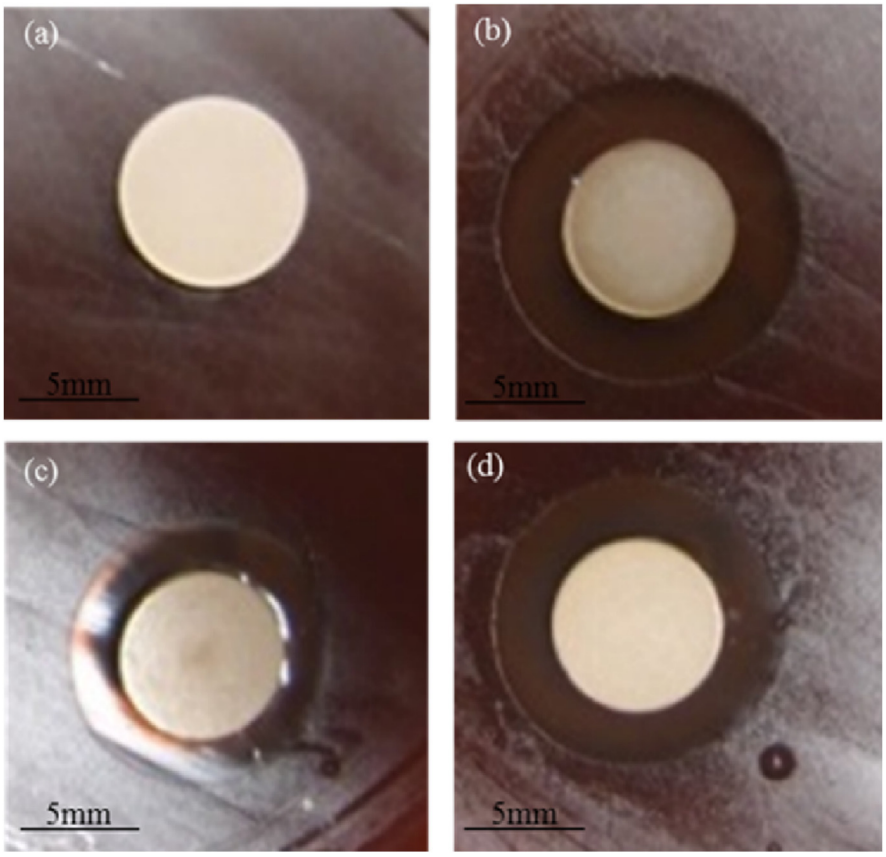

Figure 5 Disk diffusion of (a) 80S, (b) 80S/Ag1, (c) 80S/Ag5, and (d) 80S/Ag10 for A. actinomycetemcomitans.

the concentration of silver ions on agar, and the antibacterial activity, consistent with the previous finding by Martínez-Castañon et al.[18] The formation of large-sized silver particles on the outer structure of 80S/Ag5 and 80S/Ag10 might influence the contact between the mesopores and the environment, speculating that the presence of silver particles on the surface of materials might affect the silver release and the antibacterial activities.

The long-term antibacterial effect was examined by soaking the 80S/Ag materials in simulated body fluid for 24, 48, 72, and 168 h, and the immersed materials were subjected to the disk diffusion tests (Table 3). Even after prolonged immersion in simulated body fluid, 80S/Ag still exhibited significant antibacterial effects, indicating that the materials in this study possessed superior and long-lasting antibacterial functionality.

Table 2 The inhibition zone for *A. actinomycetemcomitans*. (ND, not detectable.)

Material	Mean diameter of the inhibition zone (mm)
80S	ND
80S/Ag1	16.5 ± 0
80S/Ag5	15.0 ± 0
80S/Ag10	15.0 ± 0

Remineralization of 80S/Ag in simulated body fluid

The surface morphologies of the 80S/Ag materials were captured after immersion in simulated body fluid (SBF) for 24–168 h, as shown in (Figs. 8–11). Needle-like deposits were observed on the material surface, and the accumulation of deposits became more pronounced with increasing

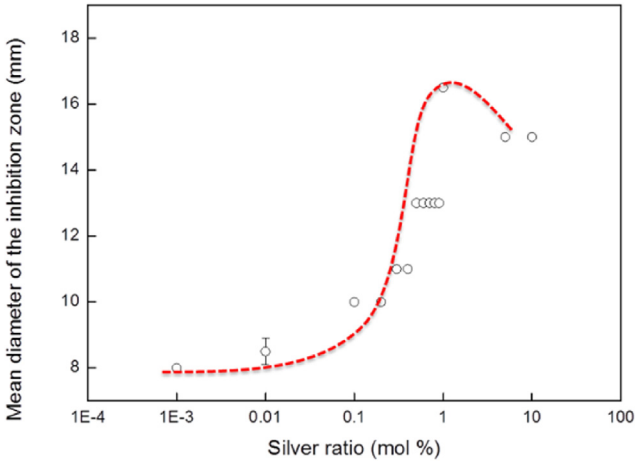

Figure 6 The dependence between the inhibition zone and different Ag concentrations against A. actinomycetemcomitans.

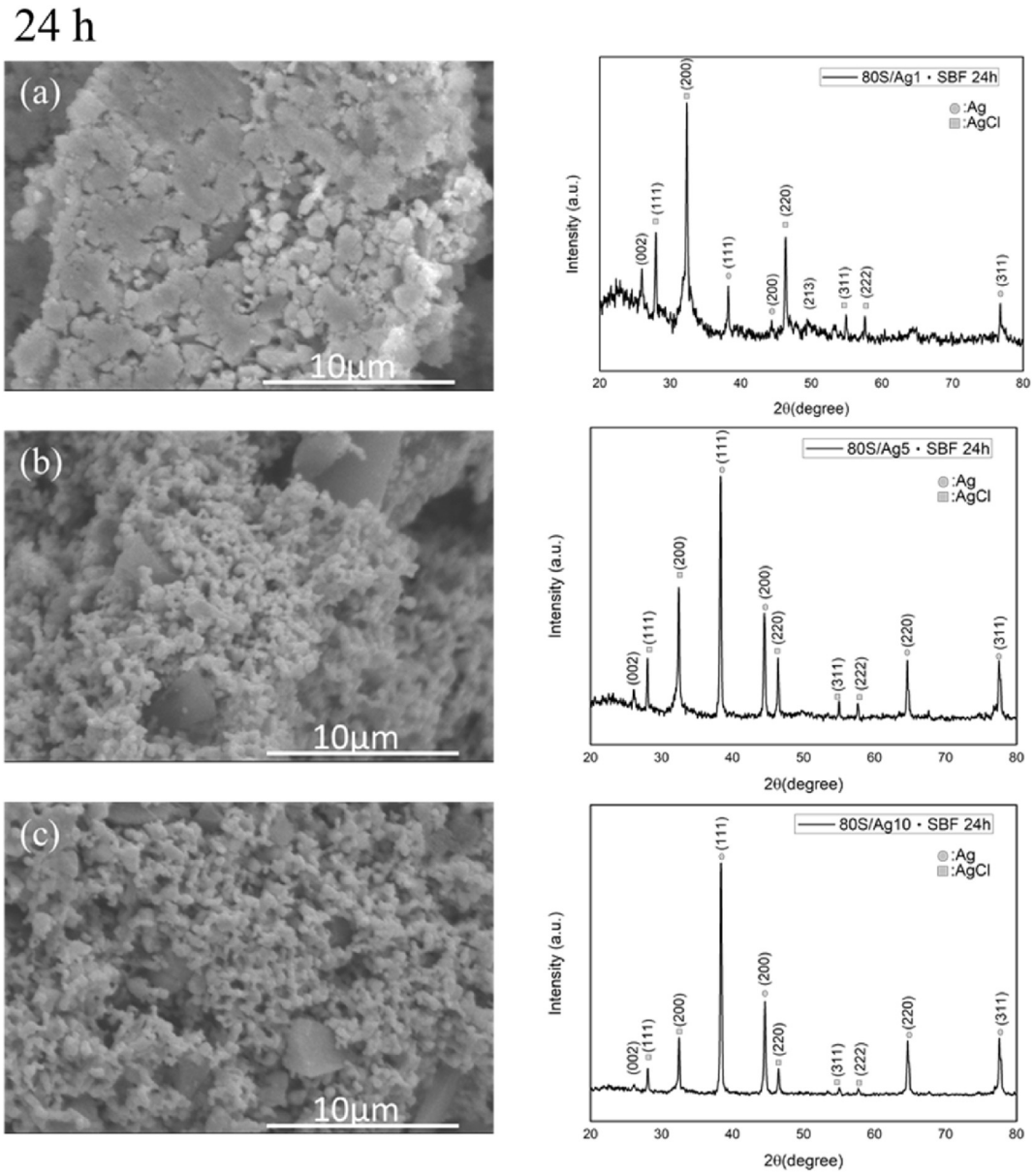

Figure 7 SEM micrographs and XRD of (a) 80S/Ag1, (b) 80S/Ag5, (c) 80S/Ag10 after being immersed in simulated body fluid (SBF) for 24 h.

time. The XRD analyses were further conducted to determine the crystalline structure of the deposits. The strong crystal peaks at 2θ values of 27.8°, 32.2°, and 46.2° corresponded for the silver crystalline, similar to the materials before immersion. Moreover, some small crystal peaks were found at 2θ values of 25.8°, 31.8°, and 49.7°, which were identified as hydroxyapatite after comparison with JCPDs. Besides, the crystals of silver chloride were noticed in the XRD spectra (Figs. 7—10). It could be speculated that the released silver was prone to precipitate with chloride ions in the simulated body fluid as silver chloride form (KSP = 1.77×10^{-10}), especially in the materials with higher silver contents (e.g. the 80S/Ag5 and 80S/Ag10). The precipitation might illustrate the reason that the antibacterial activities deceased for the 80S/Ag5 and 80S/Ag10 (Fig. 6).

Table 3 The inhibition zone after treating with the simulated body fluid (SBF). (ND, not detectable.)

Material	Mean dimeter of inhibition zone (mm) after:				
	0h	24h	48h	72h	168h
80S	ND	ND	ND	ND	ND
80S/Ag1	16.5 ± 0	14.0 ± 0	14.0 ± 0	14.0 ± 0	13.0 ± 0
80S/Ag5	15.0 ± 0	15.0 ± 0	15.0 ± 0	15.0 ± 0	14.0 ± 0
80S/Ag10	15.0 ± 0	15.5 ± 0	15.0 ± 0	15.0 ± 0	14.0 ± 0

The 80S/Ag materials mainly consist of silicon, calcium, phosphorus, and silver, and ion dissolution or deposition occurs in SBF, causing changes in the pH of the simulated

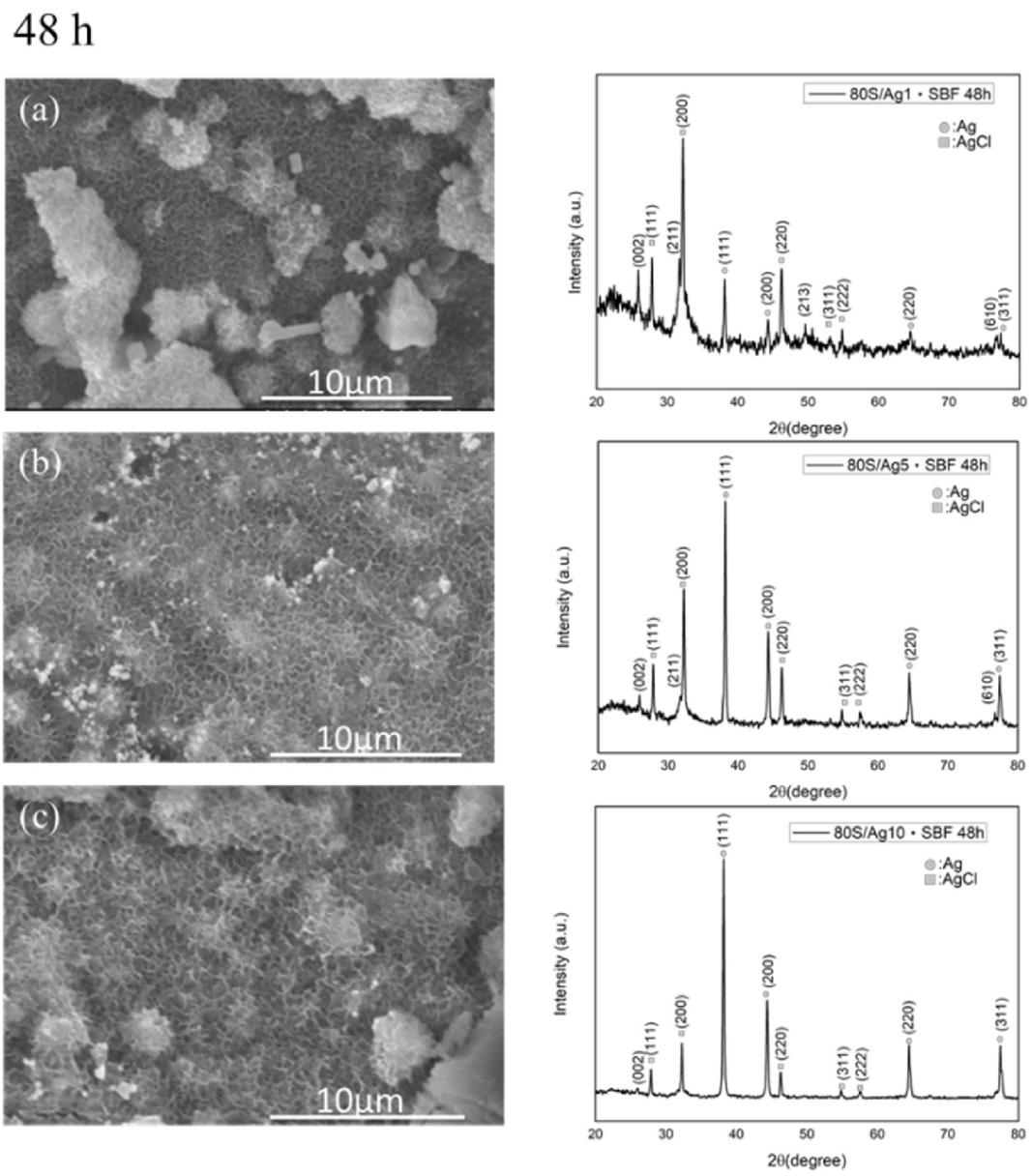

Figure 8 SEM micrographs and XRD of (a) 80S/Ag1, (b) 80S/Ag5, (c) 80S/Ag10 after being immersed in simulated body fluid (SBF) for 48 h.

body fluid. Thus, the pH values were measured after different immersion times (Fig. 11). The slightly increased pH of the simulated body fluid illustrated that the ions were released by 80S and 80S/Ag, resulting in the pH changes. The finding agreed with the previous study that the mesoporous silica-based calcium phosphate bioglass could release the silicon, calcium, and phosphate ions and, thus, increase the pH of the solution.[23]

Discussion

Nanotechnology has drawn researchers' attention in many fields and developed numerous biomedical science applications, where the silver nanoparticle as an antimicrobial agent was applied for many dental purposes.[8] Castro et al. developed a resin decorated with nanostructured silver vanadate and evaluate the influence of the material against the oral microbiota and their biofilm formation on the material.[19] Their result illustrated the difference of microbiota diversity significantly related to exposure time and concentration of the silver nanoparticle materials. Dias et al. synthesized the silver-doped ZnO nanoparticle and investigated its composite resin to different oral pathogens.[20] An anti-biofilm activity was observed for the composite resin modified by silver-doped ZnO nanoparticles, along with sufficient compressive strength. Lampé et al. demonstrated a titanium implant with long-term

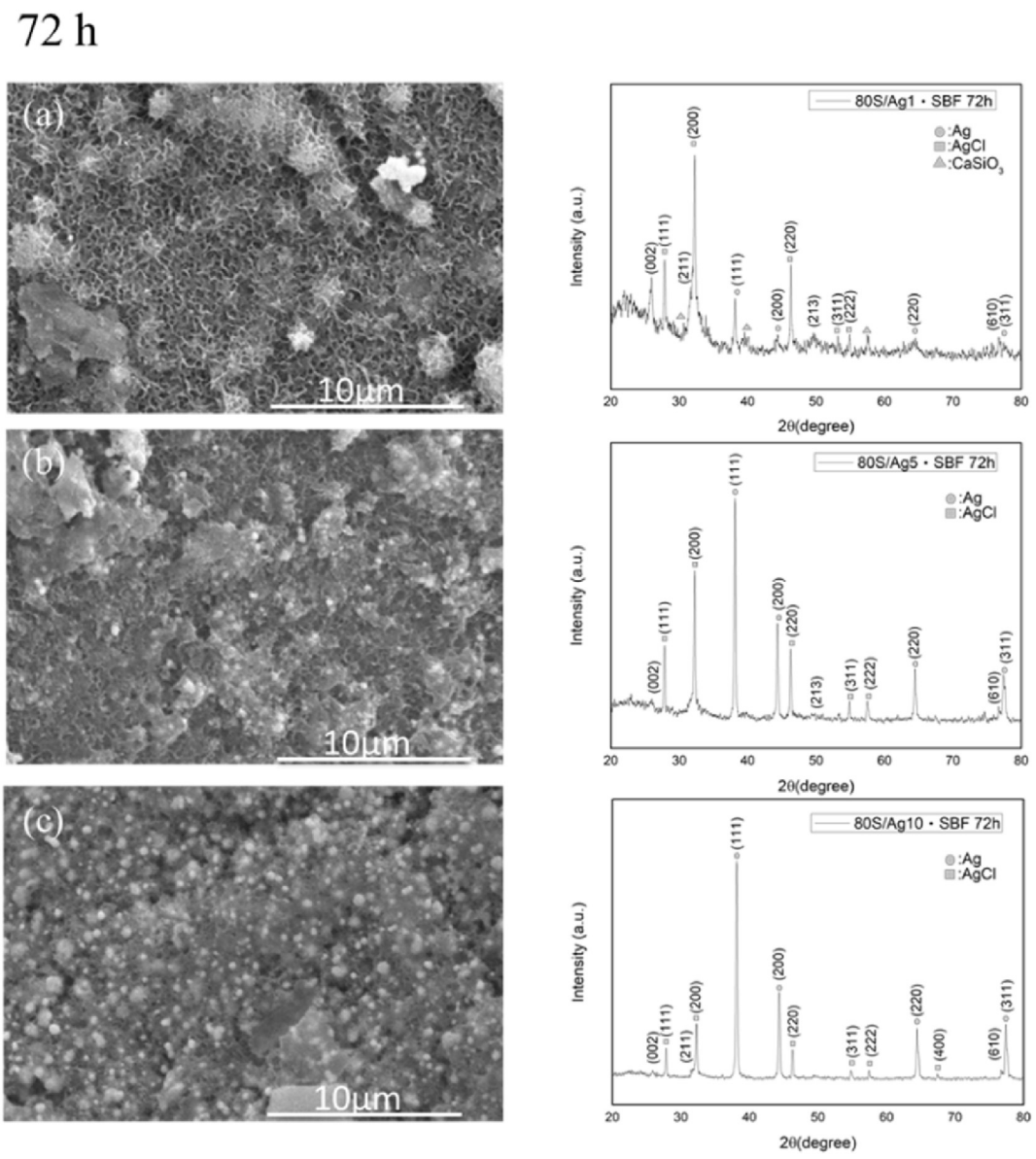

Figure 9 SEM micrographs and XRD of (a) 80S/Ag1, (b) 80S/Ag5, (c) 80S/Ag10 after being immersed in simulated body fluid (SBF) for 72 h.

antibacterial effects empowered by release-controllable silver ions.[21] The long-lasting antibacterial activity protected the implant from destruction by infections or inflammations, and the release-controllable characteristic promise low toxicity to the host. In the current work, we developed a material consisting of Si, Ca, P, and Ag, namely the 80S/Ag, to achieve a similar concept of bioactivities. The mesoporous structure of the 80S/Ag has been documented as a remarkable drug delivery system.[22] In the antibacterial testing, the 80S/Ag demonstrated antibacterial activity against the commonly-found oral pathogen, *A. actinomycetemcomitans* (Table 2 and Fig. 5), with a long-lasting effect for 168h (Table 3). The formation of hydroxyapatite in simulated body fluid highlighted the characteristic of bone and dentine remineralization for the 80S/Ag (Figs. 7—10). The simulated body fluid (SBF) method has been documented to evaluate the bone-bonding capacity and degradation processes of materials.[23] The SBF simulates the inorganic component of human blood plasma or tissue fluid,[24] able to study the leaching of metal ions from fake braces[25] or the osseointegration of titanium implants[26] and providing a non-animal alternative for evaluating the performance and safety of materials in a simulated physiological environment. Moreover, the increased pH values after immersion in simulated body fluid would help neutralize the acidic oral environment, where the bacteria damage teeth and the surrounding regions.[27] Various genes were involved in odontoblast-like cell differentiation and mineralization, namely the dentine remineralization and regeneration,[28] such as dentin matrix acidic

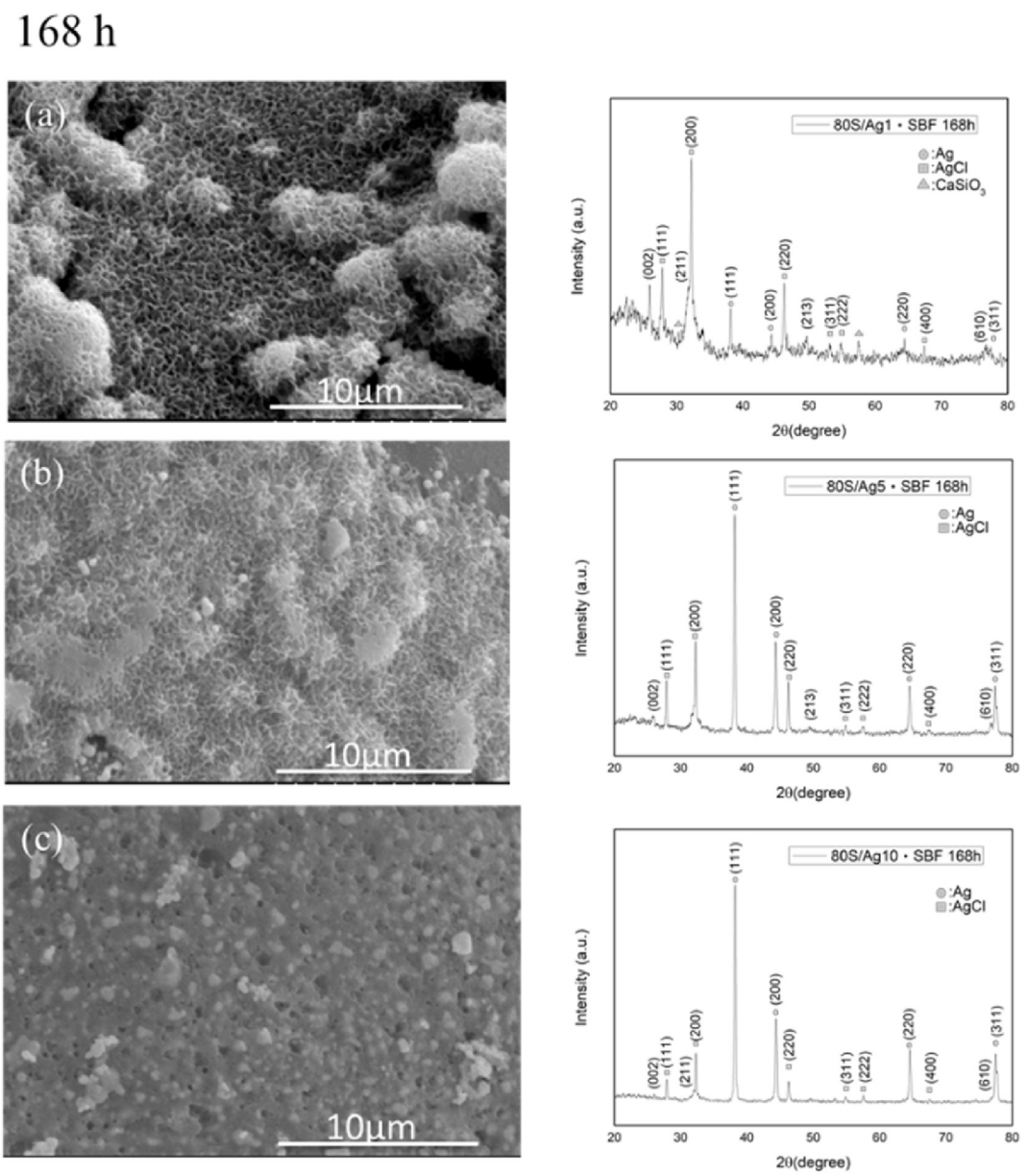

Figure 10 SEM micrographs and XRD of (a) 80S/Ag1, (b) 80S/Ag5, (c) 80S/Ag10 after being immersed in simulated body fluid (SBF) for 168 h.

phosphoprotein 1 (DSPP), dentin sialophosphoprotein (DSP), dentine matrix protein 1 (DMP-1), collagen type I alpha 1 chain (COL1A1), alkaline phosphatase (ALPL), integrin-binding sialoprotein (IBSP), bone gamma-carboxyglutamate protein (BGLAP), vascular endothelial growth factor A (VEGFA), cyclin dependent kinase inhibitor 1A (CDKN1A), *etc*. Additionally, GPC-1(glypican-1) and TGF-β1(transforming growth factor beta-1) have been reported to be related to the early stages of odontoblast-like cell differentiation,[29] with the downregulation of the GPC-1 gene observed for the formation of reparative dentine. Encouraged by these observations, the genes were considered therapeutic targets for promoting dentin regeneration.[30]

Our results indicate that 80S/Ag possesses remarkable antibacterial properties. Prolonged immersion in simulated body fluid led to hydroxyapatite formation, indicating the potential to help dentine remineralization. The long-lasting antibacterial ability and increased pH values after immersion in simulated body fluid were beneficial in dentistry. The findings in this work supported the potential therapeutic application of the 80S/Ag for treating periodontal disease. However, further work on the formulation and *in vivo* studies would be needed. Regarding the 80S/Ag in this study being in powder form, light-curing resin-based composites would be employed in a rat model where the dental structure was large enough to ease the operating limitation.

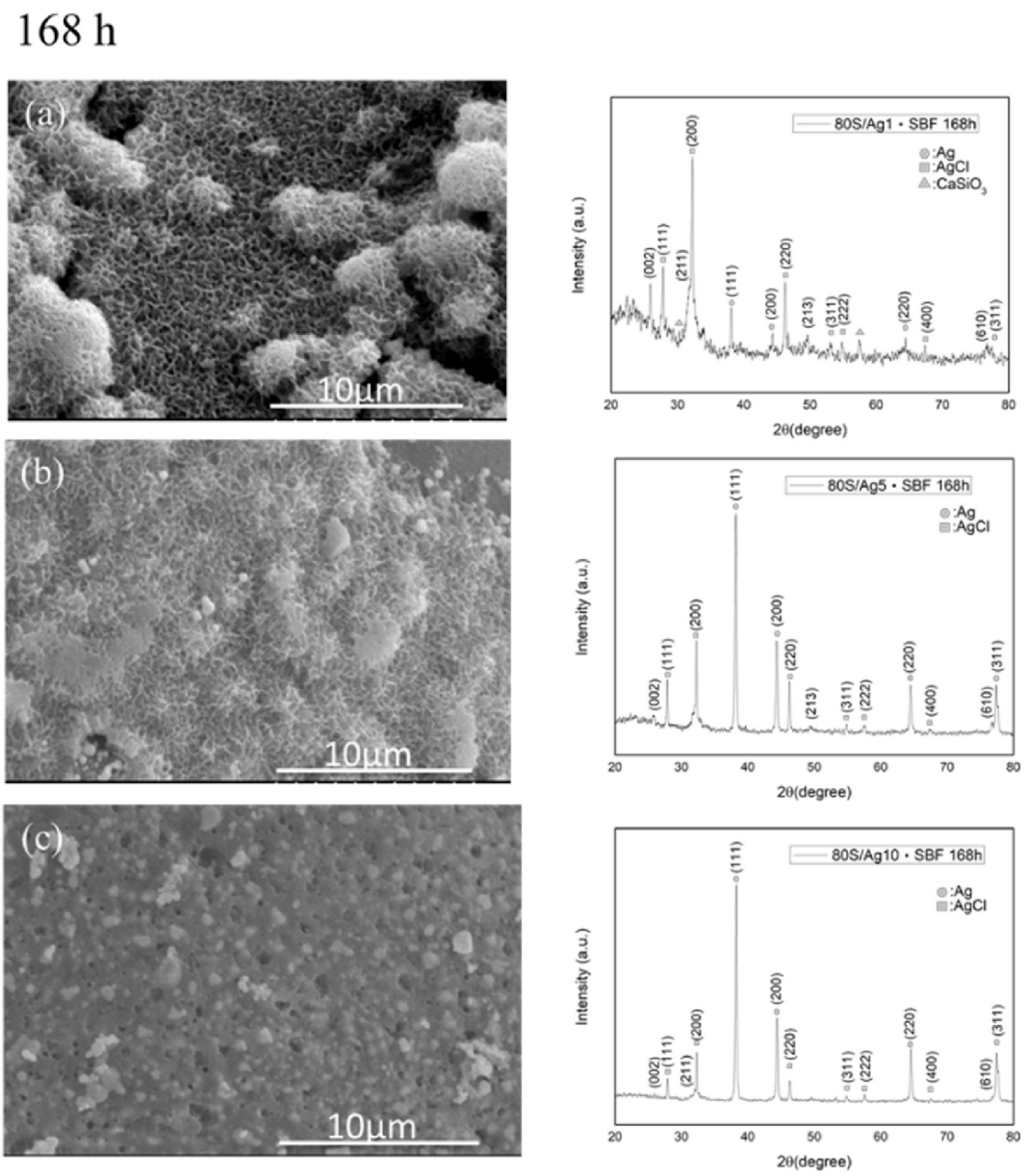

Figure 11 pH variations of SBF when 80S, 80S/Ag1, 80S/Ag5, and 80S/Ag10 after being immersed in simulated body fluid (SBF) for different time periods.

Declaration of Generative AI and AI-assisted technologies in the writing process

During the preparation of this work the authors used Grammarly in order to edit language. After using this tool/service, the authors reviewed and edited the content as needed and take full responsibility for the content of the publication.

Declaration of competing interest

The authors have no conflicts of interest relevant to this article.

Acknowledgments

This research was funded by the National Science and Technology Council, TW (MOST 111-2221-E-037-006, MOST 111-2314-B-037-047 and NSTC 112-2314-B-037-113-MY3), I-Shou University, TW (ISU-112-02-03A), and Kaohsiung Municipal Ta-Tung Hospital, TW (kmtth-111-R001).

Appendix A. Supplementary data

Supplementary data to this article can be found online at https://doi.org/10.1016/j.jds.2023.10.014.

References

1. Norskov-Lauritsen N, Claesson R, Birkeholm Jensen A, Aberg CH, Haubek D. *Aggregatibacter actinomycetemcomitans*: clinical significance of a pathobiont subjected to ample changes in classification and nomenclature. *Pathogens* 2019;8:243.
2. Kapoor A, Malhotra R, Grover V, Grover D. Systemic antibiotic therapy in periodontics. *Dent Res J* 2012;9:505—15.
3. Ardila CM, Bedoya-Garcia JA. Antimicrobial resistance of *Aggregatibacter actinomycetemcomitans*, *Porphyromonas gingivalis* and *Tannerella forsythia* in periodontitis patients. *J Glob Antimicrob Resist* 2020;22:215—8.
4. Belibasakis GN, Belstrom D, Eick S, Gursoy UK, Johansson A, Kononen E. Periodontal microbiology and microbial etiology of periodontal diseases: historical concepts and contemporary perspectives. *Periodontol 2000* 2023:1—17.
5. Zawadzki PJ, Perkowski K, Padzik M, et al. Examination of oral microbiota diversity in adults and older adults as an approach to prevent spread of risk factors for human infections. *BioMed Res Int* 2017;2017:8106491.
6. Sim W, Barnard RT, Blaskovich MAT, Ziora ZM. Antimicrobial silver in medicinal and consumer applications: a patent review of the past decade (2007-2017). *Antibiotics (Basel)* 2018;7:93.
7. Gherasim O, Puiu RA, Birca AC, Burdusel AC, Grumezescu AM. An updated review on silver nanoparticles in biomedicine. *Nanomaterials* 2020;10:2318.
8. Yin IX, Zhang J, Zhao IS, Mei ML, Li Q, Chu CH. The antibacterial mechanism of silver nanoparticles and its application in dentistry. *Int J Nanomed* 2020;15:2555—62.
9. Wang YC, Lin SH, Chien CS, Kung JC, Shih CJ. *In vitro* bioactivity and antibacterial effects of a silver-containing mesoporous bioactive glass film on the surface of titanium implants. *Int J Mol Sci* 2022;23:9291.
10. Parizi MK, Doll K, Rahim MI, Mikolai C, Winkel A, Stiesch M. Antibacterial and cytocompatible: combining silver nitrate with strontium acetate increases the therapeutic window. *Int J Mol Sci* 2022;23:8058.
11. Kung J-C, Chen Y-J, Chiang Y-C, et al. Antibacterial activity of silver nanoparticle (AgNP) confined mesoporous structured bioactive powder against *Enterococcus faecalis* infecting root canal systems. *J. Non-Cryst* 2018;502:62—70.
12. Ravikovitch PI, Neimark AV. Characterization of nanoporous materials from adsorption and desorption isotherms. *Colloids Surf A Physicochem Eng Asp* 2001;187:11—21.
13. Kokubo T, Yamaguchi S. Simulated body fluid and the novel bioactive materials derived from it. *J Biomed Mater Res* 2019;107:968—77.
14. Ullah A, Kabir MF, Akter M, et al. Green synthesis of biomolecule encapsulated magnetic silver nanoparticles and their antibacterial activity. *RSC Adv* 2018;8:37176—83.
15. Lin MC, Chen CC, Wu IT, Ding SJ. Enhanced antibacterial activity of calcium silicate-based hybrid cements for bone repair. *Mater Sci Eng C Mater Biol Appl* 2020;110:110727.
16. Gargiulo N, Cusano AM, Causa F, Caputo D, Netti PA. Silver-containing mesoporous bioactive glass with improved antibacterial properties. *J Mater Sci Mater Med* 2013;24:2129—35.
17. Thommes M. Physical adsorption characterization of nanoporous materials. *Chem Ing Tech* 2010;82:1059—73.
18. Martínez-Castañon G-A, Nino-Martinez N, Martinez-Gutierrez F, Martínez-Mendoza J, Ruiz F. Synthesis and antibacterial activity of silver nanoparticles with different sizes. *J Nanopart Res* 2008;10:1343—8.
19. de Castro DT, do Nascimento C, Alves OL, de Souza Santos E, Agnelli JAM, Dos Reis AC. Analysis of the oral microbiome on the surface of modified dental polymers. *Arch Oral Biol* 2018;93:107—14.
20. Dias HB, Bernardi MIB, Marangoni VS, de Abreu Bernardi AC, de Souza Rastelli AN, Hernandes AC. Synthesis, characterization and application of Ag doped ZnO nanoparticles in a composite resin. *Mater Sci Eng C Mater Biol Appl* 2019;96:391—401.
21. Lampe I, Beke D, Biri S, et al. Investigation of silver nanoparticles on titanium surface created by ion implantation technology. *Int J Nanomed* 2019;14:4709—21.
22. Mancilla-De-la-Cruz J, Rodriguez-Salvador M, An J, Chua CK. Three-dimensional printing technologies for drug delivery applications: processes, materials, and effects. *Int J Bioprint* 2022;8:622.
23. Groeger S, Meyle J. Reactivity of titanium dental implant surfaces in simulated body fluid. *ACS Appl Bio Mater* 2021;4:5575—84.
24. Haleem R, Shafiai NAA, Noor S. Metal ions leachables from fake orthodontic braces incubated in simulated body fluid. *BMC Oral Health* 2021;21:507.
25. Suchy T, Bartos M, Sedlacek R, et al. Various simulated body fluids lead to significant differences in collagen tissue engineering scaffolds. *Materials* 2021;14:4388.
26. Baino F, Yamaguchi S. The use of simulated body fluid (SBF) for assessing materials bioactivity in the context of tissue engineering: review and challenges. *Biomimetics* 2020;5:57.
27. Kianoush N, Adler CJ, Nguyen KA, Browne GV, Simonian M, Hunter N. Bacterial profile of dentine caries and the impact of pH on bacterial population diversity. *PLoS One* 2014;9:e92940.
28. Sulistyowati I, Sukpaita T, Limjeerajarus CN, Ampornaramveth RS. Hydroxamate-based histone deacetylase inhibitors as potential mediators to induce dentine regeneration by human dental pulp cell. *Front Dent Med* 2021;2:765462.
29. Liu MM, Li WT, Xia XM, Wang F, MacDougall M, Chen S. Dentine sialophosphoprotein signal in dentineogenesis and dentine regeneration. *Eur Cell Mater* 2021;42:43—62.
30. Nakashima M, Iohara K, Zheng L. Gene therapy for dentin regeneration with bone morphogenetic proteins. *Curr Gene Ther* 2006;6:551—60.